Parkin absence accelerates microtubule aging in dopaminergic neurons

Daniele Cartelli [a],[*],[1], Alida Amadeo [a],[1], Alessandra Maria Calogero [a],[1], Francesca Vittoria Marialuisa Casagrande [a], Carmelita De Gregorio [a], Mariarosa Gioria [a], Naoko Kuzumaki [b],[2], Ilaria Costa [a], Jenny Sassone [c], Andrea Ciammola [d], Nobutaka Hattori [e], Hideyuki Okano [b], Stefano Goldwurm [f], Laurent Roybon [g],[h], Gianni Pezzoli [f], Graziella Cappelletti [a],[i],[**]

[a] Department of Biosciences, Università degli Studi di Milano, Milano, Italy
[b] Department of Physiology, Keio University School of Medicine, Tokyo, Japan
[c] Division of Neuroscience, San Raffaele Scientific Institute and Vita-Salute University, Milano, Italy
[d] Department of Neurology and Laboratory of Neuroscience, IRCCS Istituto Auxologico Italiano, Cusano Milanino, MI, Italy
[e] Department of Neurology, Juntendo University School of Medicine, Tokyo, Japan
[f] Parkinson Institute, ASST G.Pini-CTO, ex ICP, Milano, Italy
[g] Stem Cell laboratory for CNS Disease Modeling, Wallenberg Neuroscience Center, Department of Experimental Medical Science, Lund University, BMC A10, Lund, Sweden
[h] Strategic Research Area MultiPark and Lund Stem Cell Center, Department of Experimental Medical Science, Lund University, Lund, Sweden
[i] Center of Excellence of Neurodegenerative Diseases, Università degli Studi di Milano, Milano, Italy

ARTICLE INFO

ABSTRACT

Loss-of-function caused by mutations in the parkin gene (PARK2) lead to early-onset familial Parkinson's disease. Recently, mechanistic studies proved the ability of parkin in regulating mitochondria homeostasis and microtubule (MT) stability. Looking at these systems during aging of PARK2 knockout mice, we found that loss of parkin induced an accelerated (over)acetylation of MT system both in dopaminergic neuron cell bodies and fibers, localized in the substantia nigra and corpus striatum, respectively. Interestingly, in PARK2 knockout mice, changes of MT stability preceded the alteration of mitochondria transport. Moreover, in-cell experiments confirmed that loss of parkin affects mitochondria mobility and showed that this defect depends on MT system as it is rescued by paclitaxel, a well-known MT-targeted agent. Furthermore, both in PC12 neuronal cells and in patients' induced pluripotent stem cell–derived midbrain neurons, we observed that parkin deficiencies cause the fragmentation of stable MTs. Therefore, we suggest that parkin acts as a regulator of MT system during neuronal aging, and we endorse the hypothesis that MT dysfunction may be crucial in the pathogenesis of Parkinson's disease.

© 2017 Elsevier Inc. All rights reserved.

1. Introduction

The PARK2 gene encodes for parkin, whose mutations are tightly associated with neurodegeneration and lead to early-onset familial Parkinson's disease (PD), known as autosomal recessive juvenile parkinsonism (OMIM #600116; Lesage and Brice, 2009). Parkin is an ubiquitin-E3-ligase (Shimura et al., 2000) involved in the degradation of misfolded and damaged proteins through the ubiquitin-proteasome system and, thus, in maintaining the protein homeostasis, whose failure plays a major role in aging and age-related disease (Toyama and Hetzer, 2013). Therefore, it is not surprising that parkin interacts with 2 cellular systems, which require a constant turnover and are reasonably implicated in PD pathogenesis: mitochondria (Knott et al., 2008) and microtubules (MTs) (Cartelli and Cappelletti, 2017).

It is largely accepted that parkin has the ability to control mitochondrial homeostasis, including biogenesis and degradation, as well as mitochondrial dynamics (Scarffe et al., 2014). The phosphatase and tensin homolog (PTEN)-induced putative kinase 1 (PINK1)/parkin pathway acts upstream of mitofusin (MFN) inducing

* Corresponding author at: Department of Biosciences, Università degli Studi di Milano, Via Celoria 26, Milano 20133, Italy. Tel.: +39 3334920793.
** Corresponding author at: Department of Biosciences, Università degli Studi di Milano, Via Celoria 26, Milano 20133, Italy. Tel.: +39 0250314752; fax: +30 0250315044.
E-mail addresses: daniele.cartelli@gmail.com (D. Cartelli), graziella.cappelletti@unimi.it (G. Cappelletti).
[1] These authors contributed equally to the work.
[2] Present address: Department of Pharmacology, Hoshi University, Pharmacy and Pharmaceutical Sciences, Tokyo 142-8501, Japan.

mitochondrial fusion. The same pathway regulates the transport of mitochondria, promoting the docking of damaged ones before their degradation (Wang et al., 2011). Although parkin was recently implicated in the initiation of local mitophagy in the distal axon (Ashrafi et al., 2014), in induced pluripotent stem cell (iPSC)—derived human neurons, parkin was not sufficient to initiate mitophagy (Rakovic et al., 2013). Therefore, it is unclear whether parkin plays this latter role under physiological conditions and if it is relevant during aging or PD pathogenesis (Grenier et al., 2013). Nevertheless, whether parkin can affect mitochondrial aging has been addressed. Parkin overexpression reduces MFN levels in aged *Drosophila*, with the concomitant changes in mitochondrial morphology and the increase in mitochondrial activity (Rana et al., 2013). Accordingly, different groups reported tissue- and age-specific mitochondrial defects in parkin knockout (KO) mice, namely the reduction in the respiratory capacity of striatal mitochondria concomitant to the increased content of glutathione, free radicals, and oxidative adducts, other than decreased levels of proteins involved in the protection from oxidative stress (Damiano et al., 2014; Palacino et al., 2004; Rodriguez-Navarro et al., 2007; Song et al., 2017). Altogether, these results evidenced how parkin impacts on mitochondria function during aging processes.

On the other hand, parkin interacts with tubulin, the building block of MTs, promoting its ubiquitination and degradation via ubiquitin-proteasome system (Ren et al., 2003), thus modulating tubulin turnover. Parkin directly binds and stabilizes MTs (Yang et al., 2005), and therefore, it is not surprising that mutations or exons' deletion in *PARK2* destabilize MTs, abolishing the ability of parkin to counteract the toxin-induced MT depolymerization, both in murine and human midbrain dopaminergic neurons (Ren et al., 2009, 2015). In agreement with these observations, we recently reported that PD-patient skin fibroblasts bearing *PARK2* mutations display a reduced MT mass and both MT-targeted pharmacological treatment and the overexpression of wild-type (WT) parkin restore control phenotype (Cartelli et al., 2012). Thus, evidence is accumulating on the failure of the parkin-mediated regulation of MTs in PD, but the potential effects of parkin on MTs during aging remain unknown. In this study, we used both in vivo and in vitro models to clarify whether parkin impacts on the aging of the MT system and MT-dependent functions in neurons. Taking advantage of *PARK2* KO mice, live-cell imaging on cultured cells, and iPSC-derived human midbrain neurons, we provide evidence that loss of parkin accelerates the aging of MT, and we suggest that this correlates to MT fragmentation and mitochondria accumulation.

2. Methods

2.1. Animals

Wild-type and *PARK2* KO (Goldberg et al., 2003) C57 black mice were purchased from Charles River (Calco, Italy) and used for all experiments. Mice were kept under environmentally controlled conditions (ambient temperature = 22 °C; humidity = 40%) on a 12-hour light/dark cycle with food and water *ad libitum*. Mice were kept in pathogen-free conditions and all procedures complied with the Italian law D.lgs 116/92 (*protocol number* 6/2013). All efforts were made to minimize suffering. Mice at different ages (2, 7, and 24 months) were sacrificed by decapitation or by transcardiac perfusion to perform biochemical or immunohistochemical analysis, respectively.

2.2. Western blot analysis

Western blot analysis was performed on protein extracts obtained from PC12 cells or mouse brain regions, accordingly to the previously reported protocols (Cartelli et al., 2010, 2013), using the following

antibodies raised against: α tubulin (mouse IgG, clone B-5-1-2; Sigma-Aldrich, Saint Louis, MO, USA); tyrosinated (Tyr) tubulin (rat IgG, clone YL 1/2; Abcam, Cambridge, UK); acetylated (Ac) tubulin (mouse IgG, clone 6-11B-1; Sigma-Aldrich); mitofusin-2 (MFN2) (rabbit IgG, clone D2D10; Cell Signaling Technology, Beverly, MA, USA); dynamin-related protein-1 (DRP-1) (rabbit IgG, clone D6C7; Cell Signaling Technology); phospho-DRP-1 (S616) (rabbit IgG, clone D9A1; Cell Signaling Technology); and VDAC1/porin (rabbit IgG; Abcam). Membranes were washed for 30 minutes and incubated for 1 hour at room temperature with horseradish peroxidase (HRP) donkey anti-mouse IgG (Pierce, Rockford, IL), HRP goat anti-rat IgG (Sigma-Aldrich), or HRP goat anti-rabbit IgG (Pierce). Immunostaining was revealed by enhanced chemiluminescence (SuperSignal West Pico Chemiluminescent; Pierce). Acquisition and quantification were performed by ChemiDoc and Image Lab software (Bio-Rad, Hercules, CA, USA).

2.3. Confocal analysis

Mice were anesthetized with chloralium hydrate (320 mg/kg, intraperitoneal) and transcardially perfused with 4% paraformaldehyde (PFA) in 0.1 M phosphate buffer (PB), pH 7.4. Brains were removed and postfixed 3 hours in 4% PFA. Sagittal sections (50-μm thick) were cut with a vibratome (VT1000S; Leica Microsystems, Heidelberg, Germany), and part of them was cryoprotected for long-term conservation at −20 °C. Sections were stained with the following antibodies: Tyr tubulin rat IgG (clone YL 1/2; Abcam); Ac tubulin mouse IgG (Sigma-Aldrich); and VDAC1/porin rabbit IgG (Abcam). To identify dopaminergic neurons and fibers, each section was concurrently stained with anti-tyrosine hydroxylase (TH) antibody, made in mice (clone LCN1; Millipore, Darmstadt, Germany) or rabbits (Millipore) as appropriate. As secondary antibodies, we used Alexa Fluor 568 donkey anti-mouse IgG, Alexa Fluor 488 goat anti-rabbit IgG, and Alexa Fluor 568 donkey anti-rat IgG (Invitrogen, Waltham, MA, USA). Samples were examined with a confocal laser scan microscope imaging system (TCS SP2 AOBS; Leica Microsystems) equipped with Ar/Ar-Kr 488, 561, and 405 nm diode lasers. Photomultiplier gain for each channel was adjusted to minimize background noise and saturated pixels, and once defined for control conditions, parameters were kept constant for all acquisitions. Images were acquired in different brain regions, namely the *corpus striatum*, the *substantia nigra*, and the *nigrostriatal pathway*. To estimate the overlapping area between red and green signals, analyses were carried out on single-plane raw images, and Manders' coefficients were calculated applying the JACoP plug-in (developed and reviewed by Bolte and Cordelières, 2006) for ImageJ software. Quantification of the mean fluorescence intensity inside dopaminergic neurons was performed using the appropriate module of the NIH ImageJ software. Only somas in which the nucleus was clearly evident have been selected for the analyses, and the perimeter was manually drawn. To evaluate the mitochondria distribution, the porin signal was superimposed on dopaminergic fibers, using the Mask tool of the Leica Confocal Software (Leica); mitochondria accumulations were identified as white pixel—containing areas, as thick as long, clearly separated from other white pixels as previously reported (Cartelli et al., 2013). In addition, the mitochondria accumulation was validated by the analysis of fluorescence profiles of TH and porin signals inside single dopaminergic fiber, which clearly allow distinguishing homogeneous and clustered distribution of the porin signal (Fig. S2A, arrows). A TH-positive signal longer than 5 μm was considered as dopaminergic fiber, and signals separated by more than 10 μm were counted as 2 distinct fibers.

2.4. Immunoelectron microscopy

Seven months' old mice were perfused with 4% PFA and 0.5% glutaraldehyde in 0.1 M PB as described for confocal analysis. The

vibratome sagittal sections were incubated sequentially with anti-TH rabbit IgG (Millipore), biotinylated goat anti-rabbit IgG (Vector Laboratories, Burlingame, CA, USA), and avidin-biotinylated peroxidase complex (ABC method, Vector Laboratories). After completion of the immune-enzymatic procedure, the visualization of reaction was performed using a solution of 0.075% 3-3′-diaminobenzidine tetrahydrochloride (DAB; Sigma-Aldrich) and 0.002% H_2O_2 in 0.05 M Tris-HCl buffer, pH 7.6, as chromogen. Next, the sections were washed in PB, osmicated, dehydrated, and flat embedded in Epon-Spurr resin between acetate foils (Aclar; Ted Pella, Redding, CA, USA). Selected areas of the embedded sections were then cut with a razor blade and glued to blank blocks of resin for further sectioning. Thin sections (70 nm) were obtained with an ultramicrotome (Reichert UltraCut E; Leica Microsystems) and observed with the Philips CM10 transmission electron microscope at 80 kV; images were acquired using the Morada Olympus digital camera. The acquired images include both longitudinal and transversal sections of dopaminergic fibers. We carried out the following rough quantitative analyses on these sections: (1) estimation of the percentage of the fiber including 1, 2, or more than 2 mitochondria clustered along the thickness of the fiber and (2) evaluation of the axon dimension, both in term of area in transversal sections and in term of thickness in longitudinal sections. The perimeter of the measured axons was manually drawn and the analyses were performed using the appropriate module of the NIH ImageJ software.

2.5. Live-cell imaging

PC12 cells were maintained in cultures and differentiated for 3 days with nerve growth factor, (NGF; Cartelli et al., 2010). PC12 cells were parkin silenced using Lipofectamine 2000 (Invitrogen) (1:3 DNA to Lipofectamine ratio) with the shRNA previously described (Helton et al., 2008; Maraschi et al., 2014), which contains green fluorescence protein as reporter, and co-transfected with either EB3-mCherry construct (Cartelli et al., 2016) or Mito-DsRed (Cartelli et al., 2010). Three days after transfection, cultures were transferred to a live-cell imaging workstation composed of an inverted microscope (Axiovert 200 M; Zeiss, Oberkochen, Germany), a heated (37 °C) chamber (Okolab, Naple, Italy), and a Plan neofluar 63×/1.25 numerical aperture oil-immersion objective (Zeiss). Images were collected with a cooled camera (Axiocam HRM Rev. 2; Zeiss), every 6 seconds for the analyses of MT growth and every 10–15 seconds for mitochondrial trafficking; single movie duration was set at 1–3 minutes, and the total recording time did not exceed 60 minutes for each dish. For rescue experiments, cells were incubated for 2 hours with 1 μM paclitaxel (Sigma-Aldrich) dissolved in methanol. MT growth dynamics was analyzed from EB3 time-lapse movies using the plusTipTracker software (Applegate et al., 2011), whereas mitochondrial movement was analyzed by the Imaris software, kindly provided by Immagini & Computer (Bareggio, Italy). Silenced cells were fixed and stained as already reported (Cartelli et al., 2010) and analyzed by a confocal microscope.

2.6. Generation and differentiation of human iPSCs

The generation and differentiation of iPSC lines B7, WD, PA7 and PB2, and CSC-9A and CSC-7A was reported elsewhere (Holmqvist et al., 2016; Imaizumi et al., 2012). Differentiated cells, aged day 30 + 7, were stained with anti-Ac tubulin mouse IgG (Sigma-Aldrich), anti-Tyr tubulin rat IgG, and anti-TH rabbit IgG. As secondary antibodies, we used Alexa Fluor 568 donkey anti-mouse IgG, Alexa Fluor 647 donkey anti-rat IgG (Abcam), and Alexa Fluor 488 goat anti-rabbit IgG. Samples were examined with a confocal laser scan microscope imaging system (TCS SP5; Leica Microsystems), and Ac-staining fragmentation was analyzed with ImageJ software. Thus, we used 2 sets of iPSC lines,

generated in 2 different laboratories using 2 different protocols and bearing different parkin mutations as exon deletions (PA7: exon 2–4 homozygous deletion of *PARK2* gene and PB2: exon 6,7 homozygous deletion of *PARK2* gene, from the Okano's Laboratory in Japan) or a point mutation (CSC-7A: C253Y located in exon 7 of *PARK2* gene, from the Roybon's Laboratory in Sweden).

2.7. Statistical analysis and data management

The statistical significance of genetic background or treatment was assessed by Student's *t*-test, one-way analysis of variance with Fisher's least significant difference *post hoc* testing or χ^2 test when appropriate. Analyses were performed using STATISTICA software (StatSoft Inc, Tulsa, OK, USA).

3. Results

3.1. Parkin absence leads to the MT hyperacetylation in mice

To investigate whether the absence of parkin impacts on MT system during the aging of dopaminergic neurons, we evaluated MT stability in *corpus striatum* and *substantia nigra* of WT and *PARK2* KO mice at different ages, ranging from 2 months' young adult to 24 months' old mice. We examined Tyr tubulin and Ac tubulin, which are respectively associated to dynamic and stable MTs (Janke, 2014). Biochemical analyses showed that these modifications change over time in *PARK2* KO mice (Fig. S1); we observed a great variability, which we attributed to the multiple cell types (i.e., glial cells or different neuronal subpopulations) present in the *corpus striatum* and in the *ventral mesencephalon*. To get more punctual information about the changes of α tubulin post-translational modifications (PTMs) inside dopaminergic neurons, we performed immunohistochemistry and analyzed the stainings by confocal microscopy. At first, we evaluated the distribution of Tyr tubulin and Ac tubulin in the *corpus striatum* of *PARK2* KO mice (Fig. 1A, red signals); next, to uncover whether the observable changes of these tubulin PTMs could be attributed to dopaminergic terminals (Fig. 1A, green signal), we used the Manders' parameters (Fig. 1B and C), which are a reliable tool to accurately analyze signal distribution and colocalization (Bolte and Cordelières, 2006). Dopaminergic terminals of *PARK2* KO mice showed an early decrease of Tyr tubulin, the most dynamic MT pool, which was further exacerbated over time. On the other hand, we observed the early accumulation of stable MTs inside dopaminergic fibers, which is highlighted by the increased colocalization between Ac tubulin and TH signals. Looking at the fitting curves (Fig. 1B and C), we observed that the trend of α tubulin PTMs changing over time was significantly different in *PARK2* KO when compared to WT mice, suggesting that the absence of parkin impacts on MT stability and its changes during aging.

Interestingly, we observed a similar scenario when analyzing the cell body of dopamine neurons in the *substantia nigra* (Fig. 2A–C). Indeed, confocal analyses and quantification of fluorescence intensity inside dopaminergic neurons showed an early and specific accumulation of Tyr tubulin in *PARK2* KO mice, which subsequently dropped down, as highlighted by the fitting curve in Fig. 2B. On the contrary, Ac tubulin was found reduced in dopaminergic neurons of young *PARK2* KO mice, whereas it is increased by 2-fold at 24 months of age compared to WT mice (Fig. 2C; reported values correspond to 0.0021 ± 0.00021 for WT and 0.0043 ± 0.00036 for *PARK2* KO mice at 24 months of age). As we reported for the dopaminergic terminals, our analyses of dopaminergic neuron cell bodies revealed a different trend for the changing of Tyr and Ac tubulin levels inside dopaminergic neurons in the *substantia nigra* of *PARK2* KO mice.

Taken together, our data uncover the ability of parkin to modulate α tubulin PTMs in vivo. Furthermore, our results highlight
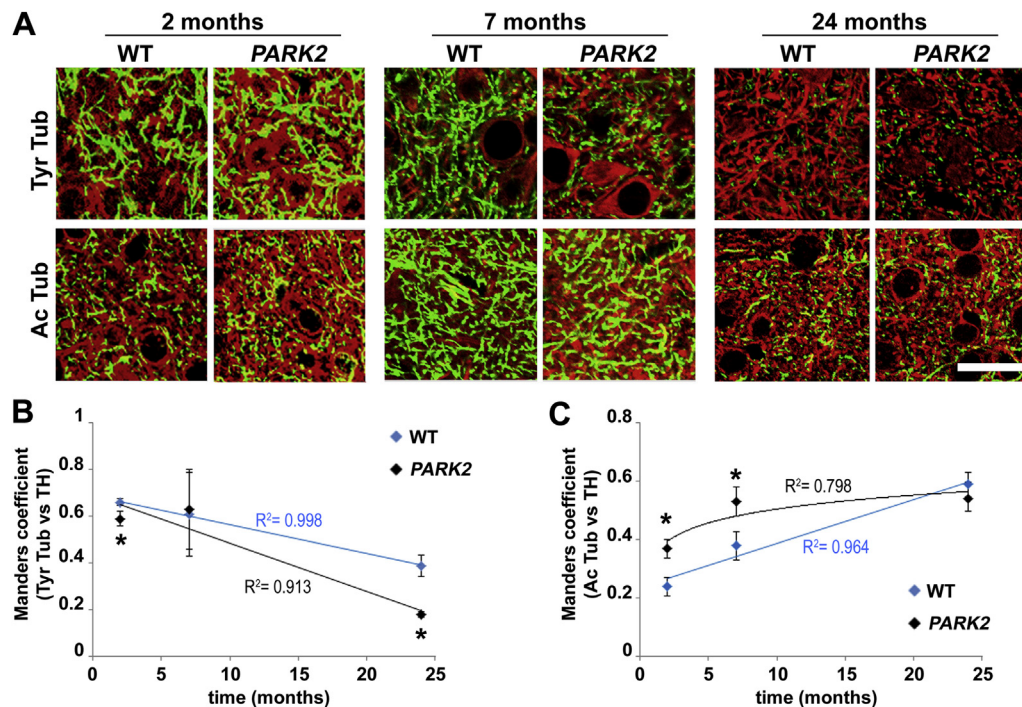
Fig. 1. Parkin absence leads to the unbalance in tubulin PTMs in the *corpus striatum*. (A) Confocal images of striatum of WT and *PARK2* knockout mice of different ages (2, 7, and 24 months). Green represents TH staining and red signals Tyr Tub or Ac Tub. Scale bar, 50 μm. (B and C) Analysis of colocalization (Manders' parameter) between Tyr Tub (B) or Ac Tub (C) and TH in striatal sections. R^2 of the linear regression of the Ac values for *PARK2* knockout mice (C, not shown) is 0.509. Data are expressed as mean ± SEM, n = 2 to 3 sections for each mouse from 3 to 4 mice per group. $^*p < 0.05$ according to Student's *t*-test. Actual *p* values are Tyr Tub, 2 months = 0.017 and 24 months = 0.0047; Ac Tub, 2 months = 0.021 and 7 months = 0.04. Abbreviations: Ac Tub, acetylated tubulin; *PARK2*, parkin gene; PTM, post-translational modification; SEM, standard error mean; TH, tyrosine hydroxylase; Tyr Tub, tyrosinated tubulin; WT, wild type. (For interpretation of the references to color in this figure legend, the reader is referred to the Web version of this article.)

that the absence of parkin affects the age-dependent changes of the MT stability. Thus, our data are intriguing as they suggest that the MT cytoskeleton inside the dopaminergic system of *PARK2* KO mice specifically and quickly loses its dynamic component, leading to accumulation of stable MTs. If this was the scenario, axons and terminals would be less prone to rapidly reorganize and less able to sustain MT-dependent process, such as axonal transport.

3.2. Parkin absence impacts on mitochondrial transport in mice

Since axonal transport is a process strictly dependent on the MT system (De Vos et al., 2008), we hypothesized that defect in the MT system induced by loss of function of *PARK2* would lead to altered mitochondrial transport. We compared the distribution of mitochondria inside dopaminergic fibers between *PARK2* KO and control mice, as we previously described (Cartelli et al., 2013). We observed dopaminergic fibers with a homogeneous distribution of mitochondria as well as fibers showing mitochondria that are sparse or clustered into varicosities (Fig. 3A and Fig. S2A). We quantified the fraction of the diverse types of fibers (Fig. 3B) and found no differences in mitochondria distribution in 2-month-old mice, whereas fibers with mitochondria clustering significantly increased in *PARK2* KO mice starting from 7 months of age. Mirroring the events we described for α tubulin PTMs, the accumulation of mitochondria clusters is fitted by different regression curves in WT and *PARK2* KO mice (Fig. 3B), thus indicating that parkin absence could affect mitochondria transport during aging.

We also performed qualitative (Fig. 3C) and quantitative (Fig. S2) ultra-structural analysis of TH$^+$ fibers by pre-embedding immunocytochemistry; we observed dopaminergic axons engulfed by several clustered mitochondria (Fig. 3C, arrows) or without

mitochondrial accumulation (Fig. 3C, arrowheads). Previous work from Palacino et al. (2004) reported no apparent changes in the total number or size of mitochondria in *PARK2* KO mice; our qualitative analysis confirmed that the mitochondria of both WT and *PARK2* KO mice display a normal gross morphology (Fig. 3C). Furthermore, *PARK2* KO mice displayed a higher fraction of dopaminergic fibers with 2 or more clustered mitochondria if compared with WT mice (Fig. S2B), thus strengthening the results obtained by the analyses performed on confocal microscopy images (Fig. 3B). Since these are typical signs of axonal transport impairment (De Vos et al., 2008), we wondered if there was also axonal swelling; thus, we took a look at the axon dimension (Fig. S2C) and we observed that dopaminergic fibers are thicker in *PARK2* KO mice than in WT ones. To exclude that all the reported differences in mitochondrial distribution were due to alterations of mitochondrial dynamics, we investigated well-known regulators of mitochondrial fusion and fission (Knott et al., 2008), namely MFN2, DRP-1 and its fission-promoting phosphorylation on serine 616 (Fig. S3). Since we did not observe any significant change in the levels of these proteins between WT and *PARK2* KO mice at the ages studied, we gathered that the absence of parkin did not impair mitochondrial fusion and fission processes, at least in our in vivo model, and turned toward the analysis of MTs as prospective system responsible for the changes in distribution of mitochondria due to failure of axonal transport in *PARK2* KO old mice.

3.3. Parkin regulates mitochondrial trafficking through the modulation of MT dynamics

According to the evidence we thus far accumulated and comparing the time course of the alterations reported, we
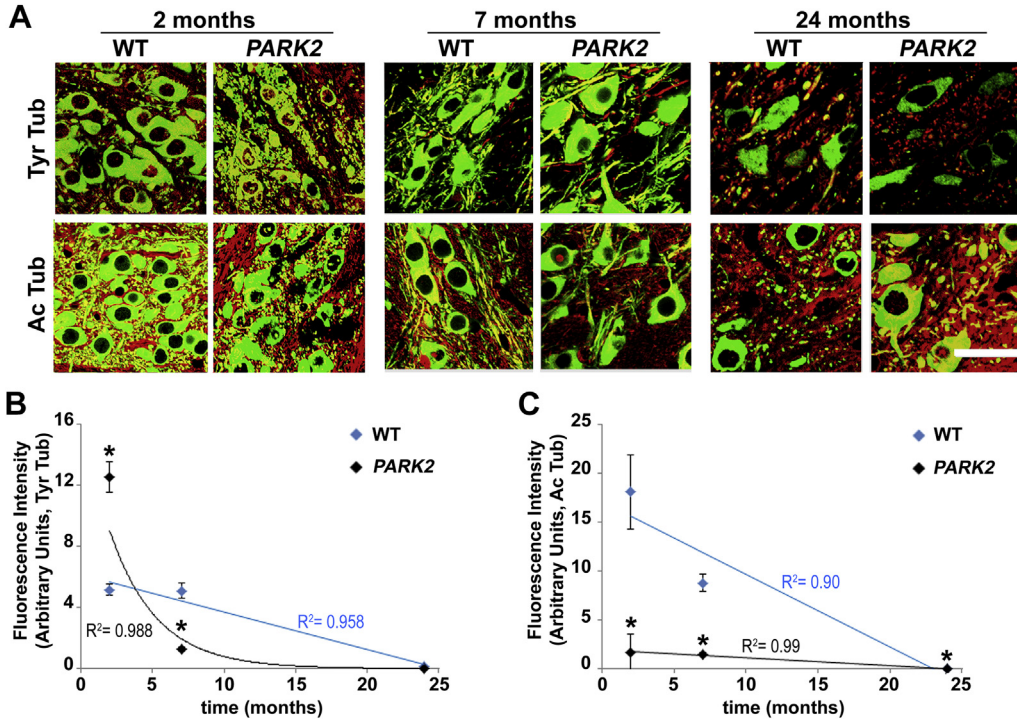
Fig. 2. Parkin absence leads to the unbalance in tubulin PTMs in the *substantia nigra*. (A) Confocal images of *substantia nigra* of WT and *PARK2* knockout mice of different ages (2, 7, and 24 months). Green represents TH staining and red signals Tyr Tub or acetylated Ac Tub. Scale bar, 50 μm. (B and C) Quantification of fluorescence of Tyr Tub (B) and Ac Tub (C) inside dopaminergic neurons in the *substantia nigra*. R^2 of the linear regression of the Tyr values for *PARK2* knockout mice (B, not shown) is 0.541. Actual values of Ac intensities in dopaminergic neurons of 24-month-old mice correspond to 0.0021 ± 0.00021 for WT and 0.0043 ± 0.00036 for *PARK2* knockout mice. Data are expressed as mean $\pm$ SEM, n = 2 to 3 sections for each mouse from 3 to 4 mice per group. $^*p < 0.05$ according to Student's *t*-test. Actual *p* values are Tyr Tub, 2 months = 0.000068 and 7 months = 0.000026; Ac Tub, 2 months = 0.000024, 7 months = 0.000026 and 24 months = 0.00006. Abbreviations: Ac Tub, acetylated tubulin; *PARK2*, parkin gene; PTM, post-translational modification; SEM, standard error mean; TH, tyrosine hydroxylase; Tyr Tub, tyrosinated tubulin; WT, wild type. (For interpretation of the references to color in this figure legend, the reader is referred to the Web version of this article.)

hypothesize that the mitochondria accumulation observed in 7-month-old *PARK2* KO mice (Fig. 3) might be directly caused by the unbalance of α tubulin PTMs (Figs. 1 and 2), which was already

noticeable in 2-month-old mice. To verify this hypothesis and to assess if parkin directly modulates MT dynamics, we carried out live-cell imaging experiments. We used parkin-silenced
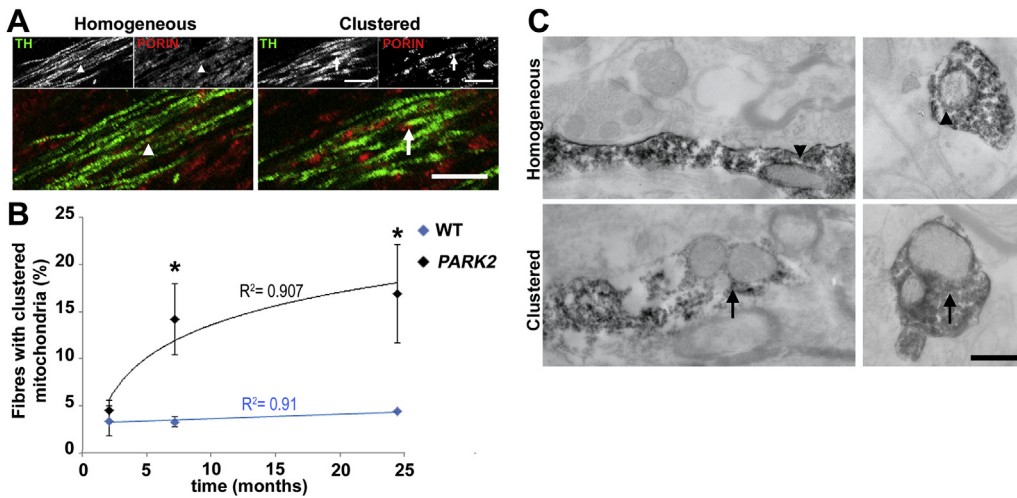

Fig. 3. Parkin absence impacts mitochondrial transport in vivo. (A) Representative confocal images showing the different distribution of mitochondria (Porin, red signal) inside dopaminergic fibers (TH, green signal). Arrowhead indicates a fiber with a homogeneous distribution of mitochondria, whereas arrow highlights a cluster. Scale bar, 20 μm. (B) Percentage of dopaminergic fibers displaying or mitochondria clustering in WT (blue) and *PARK2* knockout (black) mice of different ages (2, 7, and 24 months). R^2 of the linear regression of the values for *PARK2* knockout mice (not shown) is 0.66. Data are expressed as mean $\pm$ SEM, with more than 200 fibers analyzed per group, deriving from 3 sections for each mouse from 3 to 4 mice. $^*p < 0.05$, according to χ^2 test. The actual *p* values are 7 months = 0.000005 and 24 months = 0.0000005. (C) Electron micrographs of TH-positive fibers. Arrowheads indicate fibers with a homogeneous distribution of mitochondria, whereas arrows highlight mitochondrial clustering in both longitudinal (left) and transversal (right) sectioned dopaminergic axons. Scale bar, 500 nm. Abbreviations: *PARK2*, parkin gene; SEM, standard error mean; TH, tyrosine hydroxylase; WT, wild type. (For interpretation of the references to color in this figure legend, the reader is referred to the Web version of this article.)
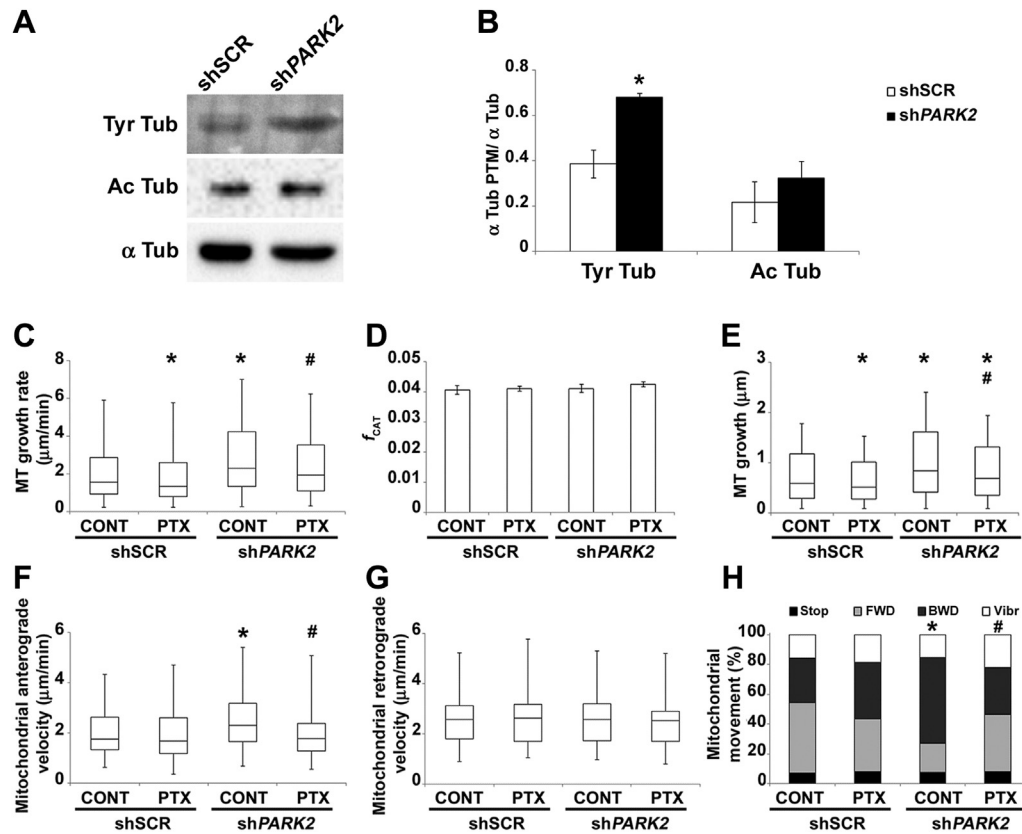
Fig. 4. Parkin modulates mitochondrial trafficking via the regulation of MT dynamics. Representative Western blot (A) and densitometric (B) analyses of Tyr Tub and Ac Tub on lysates of sh*PARK2* and shSCR NGF-differentiated PC12 cells. The level of tubulin PTMs was normalized on the level of total α Tub in the respective sample. $^*p < 0.05$, according to Student's *t*-test, performed on the rough data. Actual *p* value in B is equal to 0.0099. Box plots of the MT growth rate (C), histograms showing the f_{CAT} (D) and box plots of the MT growth displacement (E) in sh*PARK2* and shSCR NGF-differentiated PC12 cells, in basal conditions (CONT) or after 2 hours of treatment with 1 μM paclitaxel (PTX). n ≥ 1500 MTs deriving from at least 10–15 cells per experimental group. $^*p < 0.05$ versus shSCR/CONT, $^#p < 0.05$ versus sh*PARK2*/CONT according to analysis of variance, Fisher's least significant difference *post hoc* test. The actual statistical values correspond to (C) F = 40.74, $p = 0.00000001$, and the individual *p* values are shSCR/PTX versus shSCR/CONT = 0.000004, sh*PARK2*/CONT versus shSCR/CONT = 0.0000005, and sh*PARK2*/PTX versus sh*PARK2*/CONT = 0.000002; (E) F = 65.15, $p = 0.00000001$, and the individual *p* values are shSCR/PTX versus shSCR/CONT = 0.008576, sh*PARK2*/CONT versus shSCR/CONT = 0.000008, sh*PARK2*/PTX versus sh*PARK2*/CONT = 0.000008, and sh*PARK2*/PTX versus shSCR/CONT = 0.008516. Box plots of anterograde velocity (F) and retrograde velocity (G) of mitochondrial transport in sh*PARK2* and shSCR NGF-differentiated PC12 cells, in basal conditions (CONT) or after 2 hours of treatment with 1 μM paclitaxel (PTX). n ≥ 200 mitochondria tracks per condition, deriving from at least 10–15 cells per experimental group. $^*p < 0.05$ versus shSCR/CONT, $^#p < 0.05$ versus sh*PARK2*/CONT according to analysis of variance, Fisher's least significant difference *post hoc* test. The actual statistical values correspond to (F) F = 4.64, $p = 0.00033$, and the individual *p* values are sh*PARK2*/CONT versus shSCR/CONT = 0.0014 and sh*PARK2*/PTX versus sh*PARK2*/CONT = 0.00018. (H) Histogram showing the percentage of immobile mitochondria (stop, black), mitochondria forward (FWD, light gray) or backward (BWD, dark gray) moving, and vibrating mitochondria (Vibr, white) in the same conditions reported in (D) and (E). $^*p < 0.05$ versus shSCR/CONT (*p* value = 0.00025), $^#p < 0.05$ versus sh*PARK2*/CONT (*p* value = 0.0013) according to χ^2 test. Abbreviations: α Tub, α tubulin; Ac Tub, acetylated tubulin; f_{CAT}, catastrophe frequency; MT, microtubule; *PARK2*, parkin gene; PTM, post-translational modification; sh*PARK2*, parkin silenced; shSCR, scramble treated; Tyr Tub, tyrosinated tubulin.

NGF-differentiated PC12 cells (Fig. S4) expressing either EB3-mCherry, a fluorescent protein that specifically binds to a growing MT plus-end (Cartelli et al., 2016), or Mito-DsRed, which enables us to follow the movement of mitochondria (Cartelli et al., 2010). Accordingly to the data obtained in young *PARK2* KO mice, parkin-silenced PC12 cells display the significant increase of Tyr tubulin (Fig. 4A and B), which is associated with the most dynamic MTs (Janke, 2014); in agreement, live-cell data show that parkin absence significantly accelerates MT growth (Fig. 4C). Furthermore, since silencing of parkin has no effects on the frequency of MT catastrophes (Fig. 4D), it increased the MT growing distance (Fig. 4E). At the same time, absence of parkin speeded up the anterograde velocity of mitochondrial transport (Fig. 4F) with no effect on the retrograde transport (Fig. 4G). Noteworthy, silenced cells displayed a higher fraction of mitochondria moving toward the soma (Fig. 4H), meaning that the absence of parkin causes a disorientated mitochondrial trafficking. Therefore, to ascertain whether these mitochondrial motility defects were strictly related to the observed alterations in the MT system, we performed rescue experiments using the MT-stabilizing agent paclitaxel, which is able to reduce

dynamics at MT plus-ends (Ganguly et al., 2010) and to reverse alterations of axonal transport in human tau40-overexpressing rat cortical neurons (Das et al., 2014). We found that paclitaxel restored the physiological MT growth rate and, very interestingly, rescues mitochondria transport defects, correcting the direction of mitochondria movement and slowing down its velocity, in parkin-silenced PC12 cells. Altogether, our data pinpoint that parkin directly regulates MT dynamics and, in turn, modulates mitochondrial trafficking *in cells*.

3.4. *PARK2 deficiencies cause discontinuity in the acetylated MTs*

Thus far, our data showed how parkin modulates MT system in rodent experimental models, in term of tubulin PTMs and MT stability/dynamics, but transport defects can easily derive from an unusual MT morphology (De Vos et al., 2008). Therefore, we decided to investigate the organization of MTs in parkin-silenced PC12 cells (Fig. S4); in addition, to validate any possible MT-linked phenotype reminiscent of alterations in the *PARK2* gene, we look at dopaminergic neurons from iPSCs generated from *PARK2*-linked PD patients (Fig. S5). Ac tubulin
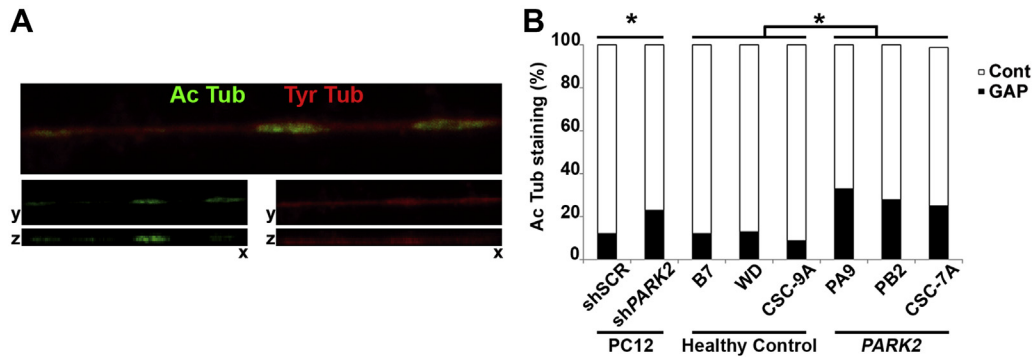
Fig. 5. Parkin deficiencies impact acetylated MTs. (A) Double staining Tyr Tub (red) and Ac tubulin (green) of a single axon. The orthogonal projections of the single channels represent x-y (top) x-z (bottom) planes and show the specificity of the gap configuration of Ac staining. (B) Histogram showing the percentage of neuronal processes with continuous (CONT, white) or gapped (GAP, black) Ac tubulin staining in sh*PARK2* and shSCR NGF-differentiated PC12 cells or control (healthy control, iPSC-lines B7, WD, CSC-9A) and patient (*PARK2*, iPSC-lines PA9, PB2, CSC-7A) iPSC-derived neurons. $^*p < 0.05$ according to χ^2 test (p values are PC12 = 0.0421 and human neurons = 0.000026). n ≥ 100 neuronal processes per experimental group (PC12) and for individual (human neurons). Abbreviations: Ac Tub, acetylated tubulin; MT, microtubule; *PARK2*, parkin gene; sh*PARK2*, parkin silenced; shSCR, scramble treated; Tyr Tub, tyrosinated tubulin. (For interpretation of the references to color in this figure legend, the reader is referred to the Web version of this article.)

staining appears discontinuous or "gapped", whereas Tyr tubulin staining seems to be continuous, even if sometimes thinner. The z−projection of the double staining of Tyr tubulin and Ac tubulin clearly reveals that the "gap configuration" is associated only to the Ac MTs (Fig. 5A), suggesting that it can be a peculiar event occurring on stable MTs, that is, MT weakening and fragmentation. A careful quantification of the neuronal processes with continuous or interrupted Ac staining highlighted the significantly higher percentage of gapped Ac MTs in parkin-silenced PC12 cells and in PD patient-derived neurons (Fig. 5B). This result was in agreement with the already reported MT destabilization in human cells (Cartelli et al., 2012; Ren et al., 2015) and highlights how parkin deficiencies specifically affect Ac MTs, suggesting the idea of a possible intrinsic weakness of MT cytoskeleton in PD patients' TH^{+} neurons where functional parkin is missing.

4. Discussion

PARK2 KO mouse model exhibits nigrostriatal deficits in the absence of nigral degeneration, and thus, it is useful for investigating early disease-related modifications and compensatory mechanisms (Goldberg et al., 2003), as well as searching for the effects of loss of parkin function (Van Rompuy et al., 2015) or the impact of parkin absence on aging process (Damiano et al., 2014; Rana et al., 2013). Here, we have first showed that parkin is involved in the regulation of the MT system in mice, reporting a specific and faster MT (over)stabilization in the dopaminergic neurons during aging of *PARK2* KO mice. Using a cell system where parkin is silenced, we further demonstrated that parkin modulates MT dynamics, whose alterations lead to the impairment of mitochondrial transport. Finally, we found that parkin deficiencies induce weakening of stable MTs both in differentiated PC12 cells and in PD patient-derived TH^{+} neurons. Thus, our data reinforce the idea that parkin impacts on MTs and indicate that it plays an important role as a modulator of the MT aging process.

Among all the data we have reported, particular attention should be paid to the effects of parkin on Ac MTs, since tubulin acetylation is a crucial controller of the aging of both MTs and brain and, in addition, it has recently been linked to neurodegeneration. It was already known that acetylation marks old MTs and that older MTs are more prone to depolymerize than younger ones (Gardner et al., 2011); furthermore, it has been proposed that α-tubulin acetyl transferase 1 (αTAT1) can act as a clock for MT lifetimes (Szyk et al., 2014), thus mediating MT aging. Very recently, it has been demonstrated that α tubulin acetylation,

which takes place on already polymerized long-lived MTs, enhances MT flexibility conferring them resilience against repeated mechanical stresses (Portran et al., 2017), the ones that an old MT has experienced during its life. In accordance with this view and to the already proposed MT-stabilizing effect of parkin (Yang et al., 2005), here we showed that *PARK2* KO mice undergo the modulation of the acetylation state of MT system, which is earlier and highly increased compared to WT mice (Figs. 1 and 2), to compensate for the absence of parkin. In case acetylation does not reach a sufficient level, Ac MTs break, as very recently demonstrated by Xu et al. (2017). This is in agreement with our data obtained in differentiated PC12 cells (Fig. S4) or in human neurons (Fig. S5), in which the nonsignificant increase of Ac tubulin correlates with a significant higher percentage of broken Ac MTs (Fig. 5), an event that could be strictly linked to the pathogenesis of PD. The short lifespan of a mouse could be not sufficient to stress enough MTs, thus inducing their breakdown; indeed, mice do not spontaneously suffer for PD. On the other hand, in the absence of functional parkin, the longer lifespan of humans may allow the full unmasking of the altered brain aging and of the pathological phenotype, which could derive from the long-lasting mechanical stress suffered by MTs and which would explain the middle/late age of onset of PD.

The beneficial potential of MT hyperacetylation does not come without detrimental side effects. Tubulin acetylation regulates axonal transport (Reed et al., 2006) and the age-dependent decrease of the activity of sirtuin 1, an MT deacetylase, leads to increased acetylation of α tubulin in aging mice, which would block axonal transport and would interfere with motor functions (Marton et al., 2010). These data are in agreement with the ones we report here, showing that mitochondrial transport impairment follows MT hyperacetylation in *PARK2* KO mice (Fig. 3) and it is rescued by an MT-stabilizer in PC12 cells (Fig. 4). The dysregulation of MT acetylation, and possibly of MT aging, is not limited to parkin-based model of PD. Indeed, MT acetylation regulates the binding of WT or mutant forms of leucine-rich repeat kinase 2 (LRRK2) (Godena et al., 2014; Law et al., 2014), which are a common cause of genetic PD, and its increased levels rescues axonal transport and locomotor deficits caused by mutations of LRRK2 (Godena et al., 2014). A similar scenario exists for the PD-inducing 1-methyl-4-phenyl-1,2,3,6-tetrahydropyridine, which induces (over)accumulation of Ac tubulin and blocks axonal transport both in cells and in mice (Cartelli et al., 2010, 2013), other than leading to Ac MTs fragmentation (Kim-Han et al., 2011). Therefore, to reach "MT rejuvenation" and to rescue impaired MT-dependent functions, it

could be useful to (re)balance the physiological level of MT acetylation through the modulation of enzymes that specifically acetylate (αTAT1) or deacetylate (HDAC6) MTs (Akella et al., 2010; Hubbert et al., 2002). To date, promising results have been obtained by regulating MT deacetylases in Huntington's disease (Dompierre et al., 2007) and PD experimental models (Godena et al., 2014; Outeiro et al., 2007).

We also analyzed the other long-lived cell system, the mitochondria, which seems to be regulated by parkin and to be involved in the pathogenesis of PD. Our work adds on to the previous accrued evidence reported by several groups (Ashrafi et al., 2014; Damiano et al., 2014; Palacino et al., 2004; Rodriguez-Navarro et al., 2007; Song et al., 2017), which did not consider the role of the MT system in mediating the effects of parkin on the control of mitochondrial homeostasis. It has been already shown that parkin modulates mitochondrial transport (Wang et al., 2011); our data reveal that parkin can exert this function in an MT-dependent manner. Our observational data strongly suggest that axonal transport impairment becomes evident later than changes in MT stability in *PARK2* KO mice, whereas live-cell imaging demonstrates that alteration of mitochondrial movement are functionally consequent to MT dysfunctions, since it is corrected by the administration of paclitaxel, a well-known MT-targeted molecule. Defects of mitochondrial motility can be indicative of mitochondrial malfunctions, and they could lead to the block of mitochondrial respiration, as well. Indeed, as others and we demonstrated, cytoskeletal-specific and PD-related toxins firstly induce significant alterations of MT system and, subsequently, a decrease in basal mitochondrial respiration (Cartelli et al., 2010; Kandel et al., 2016). Parkin is crucial also for the maintenance of mitochondrial dynamics (Scarffe et al., 2014), which is essential for modulating mitochondrial function and movement and in which MTs can participate as well (Bowes and Gupta, 2008). In concordance with the evidence that *PARK2* KO mice do not accumulate mitochondria with an abnormal morphology (Palacino et al., 2004), our qualitative ultra-structural analysis showed mitochondria with a conventional gross morphology (Fig. 3), and the biochemical approach did not reveal alteration of mitochondria fusion and fission (Fig. S3). Thus, our data suggest that parkin modulates mitochondrial transport in an MT-dependent way and that its absence does not impact on mitochondrial dynamics, at least in *PARK2* KO mice.

Altogether, our data indicate that parkin balances stable and dynamic MTs, through the regulation of tubulin PTMs, and that its deficiencies are correlated with a specific and fast MT aging. Interestingly, this would result in the mechanical breakdown of MT system, the alteration of mitochondrial transport and, likely, in mitochondrial damage and axonal degeneration. Thus, we propose that the parkin-mediated control of MT stability, and especially the modulation of tubulin acetylation, may be the Achilles' heel during aging of dopaminergic system and that its deregulation would possibly induce the PD-associated degenerative process.

Disclosure statement

Appendix A. Supplementary data

Supplementary data associated with this article can be found, in the online version, at https://doi.org/10.1016/j.neurobiolaging.2017.09.010.

References

Akella, J.S., Wloga, D., Kim, J., Starostina, N.G., Lyons-Abbott, S., Morrissette, N.S., Dougan, S.T., Kipreos, E.T., Gaertig, J., 2010. MEC-17 is an alpha-tubulin acetyl-transferase. Nature 467, 218–222.

Applegate, K.T., Besson, S., Matov, A., Bagonis, M.H., Jaqaman, K., Danuser, G., 2011. plusTipTracker: quantitative image analysis software for the measurement of microtubule dynamics. J. Struct. Biol. 176, 168–184.

Ashrafi, G., Schlehe, J.S., LaVoie, M.J., Schwarz, T.L., 2014. Mitophagy of damaged mitochondria occurs locally in distal neuronal axons and requires PINK1 and Parkin. J. Cell Biol. 206, 655–670.

Bolte, S., Cordelières, F.P., 2006. A guided tour into subcellular colocalization analysis in light microscopy. J. Microsc. 224, 213–232.

Bowes, T., Gupta, R.S., 2008. Novel mitochondrial extensions provide evidence for a link between microtubule-directed movement and mitochondrial fission. Biochem. Biophys. Res. Commun. 376, 40–45.

Cartelli, D., Aliverti, A., Barbiroli, A., Santambrogio, C., Ragg, E.M., Casagrande, F.V.M., Cantele, F., Beltramone, S., Marangon, J., De Gregorio, C., Pandini, V., Emanuele, M., Chieregatti, E., Pieraccini, S., Holmqvist, S., Bubacco, L., Roybon, L., Pezzoli, G., Grandori, R., Arnal, I., Cappelletti, G., 2016. α-Synuclein is a novel microtubule dynamase. Sci. Rep. 6, 33289.

Cartelli, D., Cappelletti, G., 2017. Microtubule destabilization paves the way to Parkinson's disease. Mol. Neurobiol. 54, 6762–6774.

Cartelli, D., Casagrande, F., Busceti, C.L., Bucci, D., Molinaro, G., Traficante, A., Passarella, D., Giavini, E., Pezzoli, G., Battaglia, G., Cappelletti, G., 2013. Microtubule alterations occur early in experimental parkinsonism and the microtubule stabilizer Epothilone D is neuroprotective. Sci. Rep. 3, 1837.

Cartelli, D., Goldwurm, S., Casagrande, F., Pezzoli, G., Cappelletti, G., 2012. Microtubule destabilization is shared by genetic and idiopathic Parkinson's disease patient fibroblasts. PLoS One 7, e37467.

Cartelli, D., Ronchi, C., Maggioni, M.G., Rodighiero, S., Giavini, E., Cappelletti, G., 2010. Microtubule dysfunction precedes transport impairment and mitochondria damage in MPP$^+$-induced neurodegeneration. J. Neurochem. 115, 247–258.

Damiano, M., Gautier, C.A., Bulteau, A.L., Ferrando-Miguel, R., Gouarne, C., Paoli, M.G., Pruss, R., Auchère, F., L'Hermitte-Stead, C., Bouillaud, F., Brice, A., Corti, O., Lombes, A., 2014. Tissue- and cell-specific mitochondrial defect in Parkin-deficient mice. PLoS One 9, e99898.

Das, V., Sim, D.A., Miler, J.H., 2014. Effect of taxoid and nontaxoid site microtubule-stabilizing agents on axonal transport of mitochondria in untransfected and ECFP-htau40-transfected rat cortical neurons in culture. J. Neurosci. Res. 92, 1155–1166.

De Vos, K.J., Grierson, A.J., Ackerley, S., Miller, C.C., 2008. Role of axonal transport in neurodegenerative diseases. Annu. Rev. Neurosci. 31, 151–173.

Dompierre, J.P., Godin, J.D., Charrin, B.C., Cordelières, F.P., King, S.J., Humbert, S., Saudou, F., 2007. Histone deacetylase 6 inhibition compensates for the transport deficit in Huntington's disease by increasing tubulin acetylation. J. Neurosci. 27, 3571–3583.

Ganguly, A., Yang, H., Cabral, F., 2010. Paclitaxel-dependent cell lines reveal a novel drug activity. Mol. Cancer Ther. 9, 2914–2923.

Gardner, M.K., Zanic, M., Gell, C., Bormuth, V., Howard, J., 2011. Depolymerizing kineins Kip3 and MCAK shape cellular microtubule architecture by differential control of catastrophe. Cell 146, 52–592.

Godena, V.K., Brookes-Hocking, N., Moller, A., Shaw, G., Oswald, M., Sancho, R.M., Miller, C.C., Whitworth, A.J., De Vos, K.J., 2014. Increasing microtubule acetylation rescues axonal transport and locomotor deficits caused by LRRK2 Roc-COR domain mutations. Nat. Commun. 5, 5245.

Goldberg, M.S., Fleming, S.M., Palacino, J.J., Cepeda, C., Lam, H.A., Bhatnagar, A., Meloni, E.G., Wu, N., Ackerson, L.C., Klapstein, G.J., Gajendiran, M., Roth, B.L., Chesselet, M.F., Maidment, N.T., Levine, M.S., Shen, J., 2003. Parkin-deficient mice exhibit nigrostriatal deficits but not loss of dopaminergic neurons. J. Biol. Chem. 278, 43628–43635.

Grenier, K., McLelland, G.L., Fon, E.A., 2013. Parkin- and PINK1-dependent mitophagy in neurons: will the real pathway please stand up? Front. Neurol. 4, 100.

Helton, T.D., Otsuka, T., Lee, M.C., Mu, Y., Ehlers, M.D., 2008. Pruning and loss of excitatory synapses by the parkin ubiquitin ligase. Proc. Natl. Acad. Sci. U. S. A. 105, 19492–19497.

Holmqvist, S., Lehtonen, S., Chumarina, M., Puttonen, K.A., Azevedo, C., Lebedeva, O., Ruponen, M., Oksanen, M., Djelloul, M., Collin, A., Goldwurm, S., Meyer, M.,

Lagarkova, M., Kiselev, S., Koistinaho, J., Roybon, L., 2016. Creation of a library of induced pluripotent stem cells from Parkinsonian patients. NPJ Parkinsons Dis. 2, 16009.

Hubbert, C., Guardiola, A., Shao, R., Kawaguchi, Y., Ito, A., Nixon, A., Yoshida, M., Wang, X.F., Yao, T.P., 2002. HDAC6 is a microtubule-associated deacetylase. Nature 417, 455–458.

Imaizumi, Y., Okada, Y., Akamatsu, W., Koike, M., Kuzumaki, N., Hayakawa, H., Nihira, T., Kobayashi, T., Ohyama, M., Sato, S., Takanashi, M., Funayama, M., Hirayama, A., Soga, T., Suematsu, M., Yagi, T., Ito, D., Kosakai, A., Hayashi, K., Shouji, M., Nakanishi, A., Suzuki, N., Mizuno, Y., Mizushima, N., Amagai, M., Uchiyama, Y., Mochizuki, H., Hattori, N., Okano, H., 2012. Mitochondrial dysfunction associated with increased oxidative stress and α-synuclein accumulation in PARK2 iPSC-derived neurons and postmortem brain tissue. Mol. Brain 5, 35.

Janke, C., 2014. The tubulin code: molecular components, readout mechanisms, and functions. J. Cell Biol. 206, 461–472.

Kandel, J., Angelin, A.A., Wallace, D.C., Eckmann, D.M., 2016. Mitochondrial respiration is sensitive to cytoarchitectural breakdown. Integr. Biol. (Camb) 8, 1170–1182.

Kim-Han, J.S., Antenor-Dorsey, J.A., O'Malley, K.L., 2011. The parkinsonian mimetic, MPP$^+$, specifically impairs mitochondrial transport in dopamine axons. J. Neurosci. 31, 7212–7221.

Knott, A.B., Perkins, G., Schwarzenbacher, R., Bossy-Wetzel, E., 2008. Mitochondrial fragmentation in neurodegeneration. Nat. Rev. Neurosci. 9, 505–518.

Law, B.M., Spain, V.A., Leinster, V.H., Chia, R., Beilina, A., Cho, H.J., Taymans, J.M., Urban, M.K., Sancho, R.M., Blanca Ramírez, M., Biskup, S., Baekelandt, V., Cai, H., Cookson, M.R., Berwick, D.C., Harvey, K., 2014. A direct interaction between leucine-rich repeat kinase 2 and specific β-tubulin isoforms regulates tubulin acetylation. J. Biol. Chem. 289, 895–908.

Lesage, S., Brice, A., 2009. Parkinson's disease: from monogenic forms to genetic susceptibility factors. Hum. Mol. Genet. 18, R48–R59.

Maraschi, A., Ciammola, A., Folci, A., Sassone, F., Ronzitti, G., Cappelletti, G., Silani, V., Sato, S., Hattori, N., Mazzanti, M., Chieregatti, E., Mulle, C., Passafaro, M., Sassone, J., 2014. Parkin regulates kainate receptors by interacting with the GluK2 subunit. Nat. Commun. 5, 5182.

Marton, O., Koltai, E., Nyakas, C., Bakonyi, T., Zenteno-Savin, T., Kumagai, S., Goto, S., Radak, Z., 2010. Aging and exercise affect the level of protein acetylation and SIRT1 activity in cerebellum of male rats. Biogerontology 11, 679–686.

Outeiro, T.F., Kontopoulos, E., Altmann, S.M., Kufareva, I., Strathearn, K.E., Amore, A.M., Volk, C.B., Maxwell, M.M., Rochet, J.C., McLean, P.J., Young, A.B., Abagyan, R., Feany, M.B., Hyman, B.T., Kazantsev, A.G., 2007. Sirtuin 2 inhibitors rescue alpha-synuclein-mediated toxicity in models of Parkinson's disease. Science 317, 516–519.

Palacino, J.J., Sagi, D., Goldberg, M.S., Krauss, S., Motz, C., Wacker, M., Klose, J., Shen, J., 2004. Mitochondrial dysfunction and oxidative damage in parkin-deficient mice. J. Biol. Chem. 279, 18614–18622.

Portran, D., Schaedel, L., Xu, Z., Théry, M., Nachury, M.V., 2017. Tubulin acetylation protects long-lived microtubule against mechanical ageing. Nat. Cell Biol. 19, 391–398.

Rakovic, A., Shurkewitsch, K., Seibler, P., Grünewald, A., Zanon, A., Hagenah, J., Krainc, D., Klein, C., 2013. Phosphatase and tensin homolog (PTEN)-induced putative kinase 1 (PINK1)-dependent ubiquitination of endogenous Parkin attenuates mitophagy: study in human primary fibroblasts and induced pluripotent stem cell-derived neurons. J. Biol. Chem. 288, 2223–2237.

Rana, A., Rera, M., Walker, D.W., 2013. Parkin overexpression during aging reduces proteotoxicity, alters mitochondrial dynamics, and extends lifespan. Proc. Natl. Acad. Sci. U. S. A. 110, 8638–8643.

Reed, N.A., Cai, D., Blasius, T.L., Jih, G.T., Meyhoferm, E., Gaertig, J., Verhey, K.J., 2006. Microtubule acetylation promotes kinesin-1 binding and transport. Curr. Biol. 16, 2166–2172.

Ren, Y., Jiang, H., Hu, Z., Fan, K., Wang, J., Janoschka, S., Wang, X., Ge, S., Feng, J., 2015. Parkin mutations reduce the complexity of neuronal processes in iPSC-derived human neurons. Stem Cells 33, 68–78.

Ren, Y., Jiang, H., Yang, F., Nakaso, K., Feng, J., 2009. Parkin protects dopaminergic neurons against microtubule-depolymerizing toxins by attenuating microtubule-associated protein kinase activation. J. Biol. Chem. 284, 4009–4017.

Ren, Y., Zhao, J., Feng, J., 2003. Parkin binds to alpha/beta tubulin and increases their ubiquitination and degradation. J. Neurosci. 23, 3316–3324.

Rodriguez-Navarro, J.A., Casarejos, M.J., Menéndez, J., Solano, R.M., Rodal, I., Gomez, A., Yébenes, J.C., Mena, M.A., 2007. Mortality, oxidative stress and tau accumulation during ageing in parkin null mice. J. Neurochem. 103, 98–114.

Scarffe, L.A., Stevens, D.A., Dawson, V.L., Dawson, T.M., 2014. Parkin and PINK1: much more than mitophagy. Trends Neurosci. 37, 315–324.

Shimura, H., Hattori, N., Kubo, S.I., Mizuno, Y., Asakawa, S., Minoshima, S., Shimizu, N., Iwai, K., Chiba, T., Tanaka, K., Suzuki, T., 2000. Familial Parkinson disease gene product, parkin, is a ubiquitin-protein ligase. Nat. Genet. 25, 302–305.

Song, L., McMackin, M., Nguyen, A., Cortopassi, G., 2017. Parkin deficiency accelerates consequences of mitochondrial DNA deletions and Parkinsonism. Neurobiol. Dis. 100, 30–38.

Szyk, A., Deaconescu, A.M., Spector, J., Goodman, B., Valenstein, M.L., Ziolkowska, N.E., Kormendi, V., Grigorieff, N., Roll-Mecak, A., 2014. Molecular basis for age-dependent microtubule acetylation by tubulin acetyltransferase. Cell 157, 1405–1415.

Toyama, B.H., Hetzer, M.W., 2013. Protein homeostasis: live long, won't prosper. Nat. Rev. Mol. Cell Biol. 14, 55–61.

Van Rompuy, A.S., Oliveras-Salva, M., Van der Perren, A., Corti, O., Van der Haute, C., Baekelandt, V., 2015. Nigral overexpression of alpha-synuclein in the absence of parkin enhances alpha-synuclein phosphorylation but does not modulate dopaminergic neurodegeneration. Mol. Neurodegener. 10, 23.

Wang, X., Winter, D., Ashrafi, G., Schlehe, J., Wong, Y.L., Selkoe, D., Rice, S., Steen, J., LaVoie, M.J., Schwarz, T.L., 2011. PINK1 and Parkin target Miro for phosphorylation and degradation to arrest mitochondrial motility. Cell 147, 893–906.

Xu, Z., Schaedel, L., Portran, D., Aguilar, A., Gaillard, J., Marinkovich, M.P., Théry, M., Nachury, M.V., 2017. Microtubules acquire resistance from mechanical breakage through intraluminal acetylation. Science 356, 328–332.

Yang, F., Jiang, Q., Zhao, J., Ren, Y., Sutton, M.D., Feng, J., 2005. Parkin stabilizes microtubules through strong binding mediated by three independent domains. J. Biol. Chem. 280, 17154–17162.